eJSE International
Electronic Journal of Structural Engineering 22(2) 2022

Response Prediction of VFPI Through Equivalent Long Period Wavelet of Near-Fault Ground Motion

H. A. Admane[1] & P. B. Murnal[2]
[1]*Department of Civil Engineering, Govt. College of Engineering, Aurangabad, Maharashtra, India – 431005*
[2]*Department of Applied Mechanics, Govt. College of Engineering, Aurangabad, Maharashtra, India– 431005*

ABSTRACT: Past research has revealed that a Variable Frequency Pendulum Isolator (VFPI) effectively controls the structural responses such as base shear and structural acceleration under far and near fault earthquakes, and that the VFPI may show excessive sliding displacement under some earthquakes having 4-6 s time-period long waves. However, the influence of the amplitude of the long period wave on the sliding displacement of VFPI is absent from previous studies owing to the difficulty of determining the amplitude of a long period earthquake wave. Therefore, the present study considered the amplitude of the long period wave of an earthquake to analyse the behaviour of the structure isolated by VFPI. For this, the most dangerous long period wave of earthquakes has been extracted in the form of noise free wavelets by using Mavroeidis and Papageorgiou proposed numerical approach. The results indicate that the noise free long period wavelet effectively represents the low frequency earthquake for the structure isolated by VFPI. It is also found out that, the VFPI shows the excessive sliding displacement for only those earthquakes which contains the peak ground displacement of long period wave more than 0.40 m. The variation in the base shear and structural acceleration of structure isolated by VFPI under various value of Frequency Variation Factor (FVF) obedience the exponential and cubic form respectively. According to this, the present research provides empirical formulas, chart, and tables to predict the structural and isolator responses by using the peak ground velocity (*PGV*) and dominating low frequency (f_d) of a near fault earthquake.

KEYWORDS: Wavelet, VFPI; Variable Curvature; Prediction of Responses; Near-Fault ground motions; Low frequency ground motions.

1. INTRODUCTION

The behaviour of structures during an earthquake mainly depends on its intensity and the dominating frequencies of that earthquake. If the structure's dominating frequencies fall in the dominating frequencies of an earthquake, then the structure can undergo severe damage. As all know, the intensity and the frequencies of any earthquake can't be controllable, but the structure may be designed in a such way that the dominating frequencies of the structure shift away from the dominating frequencies of an earthquake and reduce damage to the structure. This most practical and effective approach is known as the seismic base isolation. The best way to incorporate the base isolation in structure is to separate the superstructure from substructure by adding a sliding joint. This type of isolation techniques is called as the friction base isolator or sliding isolator.

Friction Pendulum System (FPS) is one of the most practical sliding isolator which can effectively prevent the transfer of earthquake forces from substructure to superstructure (Zayas et al. 1990) (Figure 1). The sliding surface and articulated slider are connected to the substructure and the superstructure, respectively, in this system. During sliding and non-sliding phases, the articulated slider is built such that the whole weight of the superstructure acts vertically on the spherical sliding surface of FPS. Additionally, a restoring stiffness that benefit in limiting the residual displacement is provided by the oscillatory movement of the slider on the spherical sliding surface. In practical condition, the FPS is generally designed as a long period system to alleviate the resonance between earthquake and structure. Due to that, the structure isolated by FPS may undergo resonance problem with a long-period pulse like waveform of an earthquake, such as low-frequency and near-fault ground motion (Murnal and Sinha 2002; Pranesh and Sinha 2000; Tsai et al. 2003). In order to mitigate the long period resonance, Pranesh and Sinha (Pranesh and Sinha 2000) have proposed a new sliding isolation system, called Variable Frequency Pendulum Isolator (VFPI) (Figure 1). The operation of VFPI is pretty similar to that of FPS. The only difference between them is their sliding surfaces; the FPS has a spherical sliding surface with a fixed radius, while the VFPI has an elliptical sliding surface with a major axis is a linear function of sliding displacement. The extensive analytical research on the performance of structure isolated by

VFPI under the various types of earthquakes have been carried out in last decades (Admane and Murnal 2021; Lu et al. 2004; Malu and Murnal 2014; Murnal and Sinha 2002, 2004; Panchal and Jangid 2008; Pranesh and Sinha 2000; Shaikhzadeh and Karamoddin 2016). According to analytical research, VFPI can effectively control the structural responses under far fault and near fault earthquakes as compared to other sliding isolators, but it may show excessive sliding displacement for earthquakes having higher than 4 sec long period waves (Admane and Murnal 2021).

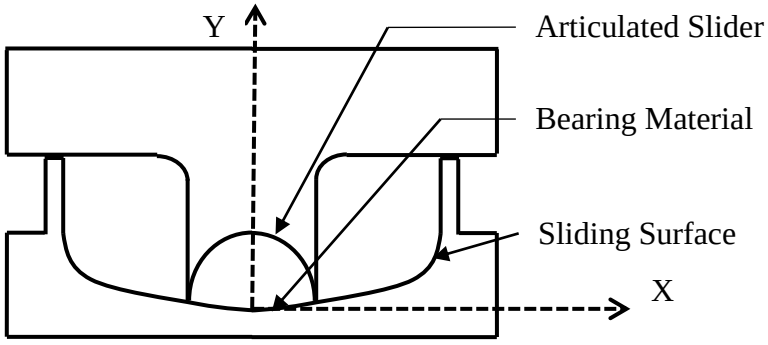

Figure 1: Schematic Diagram of Sliding Isolators.

The nature of restoring force in sliding isolators is constantly dependent on the sliding surface geometry and sliding displacement of the isolators. Typically, the primary purpose of the restoring force is to return the structure to its original position and control the sliding displacement. FPS's restoring force varies linearly with sliding displacement; hence, FPS generates a very high restoring force at high sliding displacement (Pranesh and Sinha 2000; Zayas et al. 1990). However, the restoring force of VFPI demonstrates a softening mechanism as sliding displacement increases; hence, VFPI generates just the amount of restoring force necessary to return the structure to its original position (Admane and Murnal 2021; Pranesh and Sinha 2000). Due to its shape, the restoring force generated by VFPI is much less than that of FPS. Consequently, the excessive restoring force in FPS is responsible for reducing sliding displacement and increasing structural responses under earthquake waves with long period. In the case of VFPI, however, the produced restoring force is insufficient to control the excessive sliding displacement caused by earthquake waves with long period. Due to this, VFPI under near-fault ground motions may exhibit excessive sliding displacement, and it should be considered a critical design parameter for VFPI rather than structural responses. (Admane and Murnal 2021).

As is well knowledge, a near fault earthquake may involve noises and short-period waves in addition to the most destructive long-period waves. Therefore, it is not possible to state that the responses of a structure isolated by VFPI during a near fault earthquake are only attributable to the long period wave. There is a possibility that noise and short-period waves might impact the performance of VFPI-isolated structures. In other words, the responses of a structure isolated by VFPI under two earthquakes with identical amplitudes and periods of long pulse-like waves is always distinct. Therefore, it is not generalizable to analyse the behaviour of a structure isolated by VFPI under the action of an earthquake with long-period pulse-like waves, since the result of this sort of research is restricted to the earthquake under consideration. Therefore, it is essential to extract the noise-free long period wave from an earthquake. In order to do this, Mavroeidis and Papageorgiou (Mavroeidis and Papageorgiou 2003) suggested a very effective computational method for extracting the most dangerous long period earthquake wave in the form of a noise-free wavelet. This approach extracts the noise-free long-period wavelet by closely matching the pseudo-acceleration, pseudo-velocity, and displacement response spectra of the earthquake with the retrieved noise-free wavelet.

In light of this, the current research compares the performance of a structure isolated by VFPI under the actual low frequency earthquake with its long-period noise-free wavelet (Mavroeidis and Papageorgiou 2003). The main objective of this research is to investigate the suitability of long-period noise free wavelet to replace the actual low frequency earthquake for the structure isolated by VFPI. From the performance of structure isolated by VFPI under the noise free wavelet as a ground motion, it has been found that the maximum structural responses such as the base shear and the structural acceleration follow the exponential and cubic form with respect to the Frequency Variation Factor (FVF) values of VFPI respectively. Therefore, this research also provides the empirical formulas, chart, and tables to predict the maximum base shear (V_B), the maximum absolute acceleration at top of the structure (S_a) and the maximum sliding displacement (S_d) of VFPI by using the peak ground velocity (PGV), dominating low frequency (f_d) of an earthquake and FVF. The performance of VFPI in

seismic conditions has not been investigated experimentally. Therefore, the recommendations presented in this article are tentative needing future experimental verification studies.

2. MATHEMATICAL REPRESENTATION OF DESTRUCTIVE LONG PERIOD PULSE

As discussed above, Mavroeidis and Papageorgiou (Mavroeidis and Papageorgiou 2003) have proposed a more sophisticated numerical model for representation of a destructive long-period noise free pulse from a near-fault earthquake. This numerical model was motivated from the Gabor (Gabor 1946) elementary signals, which involves four parameters: the pulse frequency, f_p, the pulse amplitude, A, phase angle, v, and the oscillatory character, γ, of the signal. According to the Mavroeidis's and Papageorgiou's numerical model, the acceleration, velocity, and displacement time history for destructive long-period pulse can be calculated by using equation (1), (2) and (3) respectively. For the calibration of the numerical model to parent near-fault earthquake, Mavroeidis and Papageorgiou have introduced a time shift, t_0, in equation (4) to precisely define the epoch of the envelope's peaks. The parameters f_p, A, v, and γ are not estimated by any formal procedure, but by a step-by-step procedure which involves judgment of the user. For instance, the pulse frequency, f_p, is determined so that the pseudo-velocity response spectra of the extracted and recorded near-fault ground motions exhibit their peak values at approximately the same natural frequency. Parameter A is determined so that the amplitude of the extracted velocity wavelet and its peak pseudo spectral velocity agree well with the corresponding quantities of the actual record, while parameters v and γ are adjusted by trial and error so as to fit the extracted velocity and displacement records with their parent earthquakes. If necessary, the minor arrangement for fitting the extracted velocity with parent earthquake can be done by readjusting parameter A.

$$\bar{a}(\bar{t}) = \frac{a(t)}{Af_p} = \begin{cases} -\frac{\pi}{\gamma}\left[\sin\left(\frac{\bar{t}}{\gamma}\right)\cos\left(\bar{t}+v\right)+\gamma\sin\left(\bar{t}+v\right)\left(1+\cos\left(\frac{\bar{t}}{\gamma}\right)\right)\right], & -\pi\gamma \le \bar{t} \le \pi\gamma \text{ with } \gamma \succ 1, \\ 0, & \text{otherwise} \end{cases} \tag{1}$$

$$\bar{v}(\bar{t}) = \frac{v(t)}{A} = \begin{cases} \frac{1}{2}\left[1+\cos\left(\frac{\bar{t}}{\gamma}\right)\right]\cos\left(\bar{t}+v\right), & -\pi\gamma \le \bar{t} \le \pi\gamma \text{ with } \gamma \succ 1, \\ 0, & \text{otherwise} \end{cases} \tag{2}$$

$$\bar{d}(\bar{t}) = \frac{d(t)}{\left(A/f_p\right)} = \begin{cases} \frac{1}{4\pi}\left[\sin\left(\bar{t}+v\right)+\frac{1}{2}\frac{\gamma}{\gamma-1}\sin\left(\frac{\gamma-1}{\gamma}\bar{t}+v\right)+\frac{1}{2}\frac{\gamma}{\gamma+1}\sin\left(\frac{\gamma+1}{\gamma}\bar{t}+v\right)\right], & -\pi\gamma \le \bar{t} \le \pi\gamma \\ \frac{1}{4\pi}\frac{1}{\left(1-\gamma^2\right)}\sin\left(v-\pi\gamma\right), & \bar{t} \prec -\pi\gamma \quad \lambda \succ 1 \\ \frac{1}{4\pi}\frac{1}{\left(1-\gamma^2\right)}\sin\left(v+\pi\gamma\right), & \bar{t} \succ -\pi\gamma \end{cases} \tag{3}$$

$$\bar{t} = 2\pi f_p\left(t-t_0\right) \tag{4}$$

The quality fitting with five different near-fault ground motion (listed in Table 1) by using the noise free wavelet has been shown in Figure 2 to Figure 6. It is evident that the numerical model proposed by Mavroeidis and Papageorgiou successfully simulates the entire set of recorded near-fault displacement, velocity, and (in some cases) acceleration time histories both qualitatively and quantitatively. But this method is meant to replicate accurately the intermediate- to long-period features of ground

motion (Mavroeidis and Papageorgiou 2003). Therefore, the difference in ground motion and elastic response spectrum of "the noise free long period wavelet" and "parent earthquake" increases with increase in frequency of the destructive long period pulse of parent earthquakes. Among the five considered near-fault ground motions, the Northridge ground motion has the high frequency destructive long period wave than the other ground motions (Table 2). Therefore, this method shows the minor difference in the ground motion and elastic response spectrum of noise free long period wavelet and parent ground motion of Northridge earthquake than others (Figure 4). From Figure 2 to Figure 6, it can also be observed that the amplitude (A) and the pulse frequency (f_p) of the extracted noise free long-period wavelet nearly matches with the peak ground velocity (PGV) and dominating low frequency (f_d) of the parent ground motion respectively. So, A and f_p can approximately replace by the PGV and f_d respectively. The parameters, which have been used to create the best fitted noise free wavelet to respective near-fault ground motion, are shown in the Table 2.

3. DESCRIPTION OF NUMERICAL MODEL AND ANALYTICAL METHOD

The primary purpose of this work is to compare an SDOF structure isolated by VFPI under actual ground motion with its noise-free long-period wavelet, as stated in the preceding section (Section 2). The mass ratio between the structure and the base is assumed to be 0.5 for this purpose. The mass and stiffness of the structure have been chosen such that the structure's fixed based time period will become 0.5 sec, while the damping ratio has been assumed to be 2% of the critical value. The isolation time period of the VFPI increases with the sliding displacement (Pranesh and Sinha 2000). This has been achieved by considering the modified equation of an ellipse as a geometric function of sliding surface of VFPI. The major axis of the modified ellipse has been taken as a linear function of the sliding displacement (equation (5)); therefore, it is geometrically equivalent to an infinite number of progressively larger ellipse merged seamlessly. The geometric function of sliding surface of the VFPI has been shown in equation (6).

$$a(x) = x + d \tag{5}$$

$$y(x) = b\left(1 - \frac{\sqrt{d^2 + 2d|x|}}{d + |x|}\right) \tag{6}$$

Where b is the minor axis of the ellipse. For VFPI, b and d are the important design parameters. Another important design parameters are the initial isolation time period (T_i) and coefficient of friction (μ), from which, the initial isolation time period at $x=0$ can be calculated from equation (7) and the coefficient of friction can be chosen from 0.02 to 0.1 (Pranesh and Sinha 2000; Shaikhzadeh and Karamoddin 2016). For this study, the VFPI chosen has the initial time period 2.0 sec and has a coefficient of friction 0.02. The variation in the isolation frequency with respect to the isolation displacement is depending on the Frequency Variation Factor, FVF $(1/d)$. Pranesh and Sinha (Pranesh and Sinha 2000) studied the performance of an SDOF structure isolated by VFPI for the 0.01 to 100 FVF values under different intensities of the El Centro Earthquake and provides the practical range of FVF from 1 to 10. Therefore, this study considered the FVF values from 1 to 10 for analysing the behaviour of SDOF structure isolated by VFPI. The impact of FVF values on the isolation frequencies have been shown in Figure 7.

Table 1: Near-Fault Record with Destructive Velocity Pulse.

Sr. No.	Location	Year	Station	Notation	Closest Fault Distance (km)	Component	Recorded PGV (m/sec)
1.	Chi-Chi, Taiwan	1999	TCU065	TCU065	0.1	EW	1.2528
2.	Tabas, Iran	1978	Tabas	Tabas	1.2	ST	1.2334
3.	Northridge, CA, USA	1994	Rinaldi	Rinaldi	8.6	S49W	1.7032
4.	Superstition Hills, CA, USA	1987	Parachute Test Site	Hill	0.7	SW	1.3422
5.	Gazli, USSR	1976	Karakyr	Gazil	3.0	NS	0.6619

Table 2: Input Parameters Obtained by Fitting the Synthetic Long-Period Pulse to Recorded Near-Fault Ground Motion.

Sr. No.	Location	A (m/sec)	γ	ν (deg)	f_p (Hz)	t_0 (s)	Notation
1.	Chi-Chi, Taiwan	1.2528	2.00	55	0.1838	29.535	TCU065-W
2.	Tabas, Iran	1.2334	2.10	00	0.1800	12.120	Tabas-W
3.	Northridge, CA, USA	1.1412	2.00	35	0.8281	02.395	Rinaldi-W
4.	Superstition Hills, CA, USA	1.3422	1.80	10	0.4910	12.090	Hill-W
5.	Gazli, USSR	0.4633	2.00	00	0.2100	07.821	Gazil-W

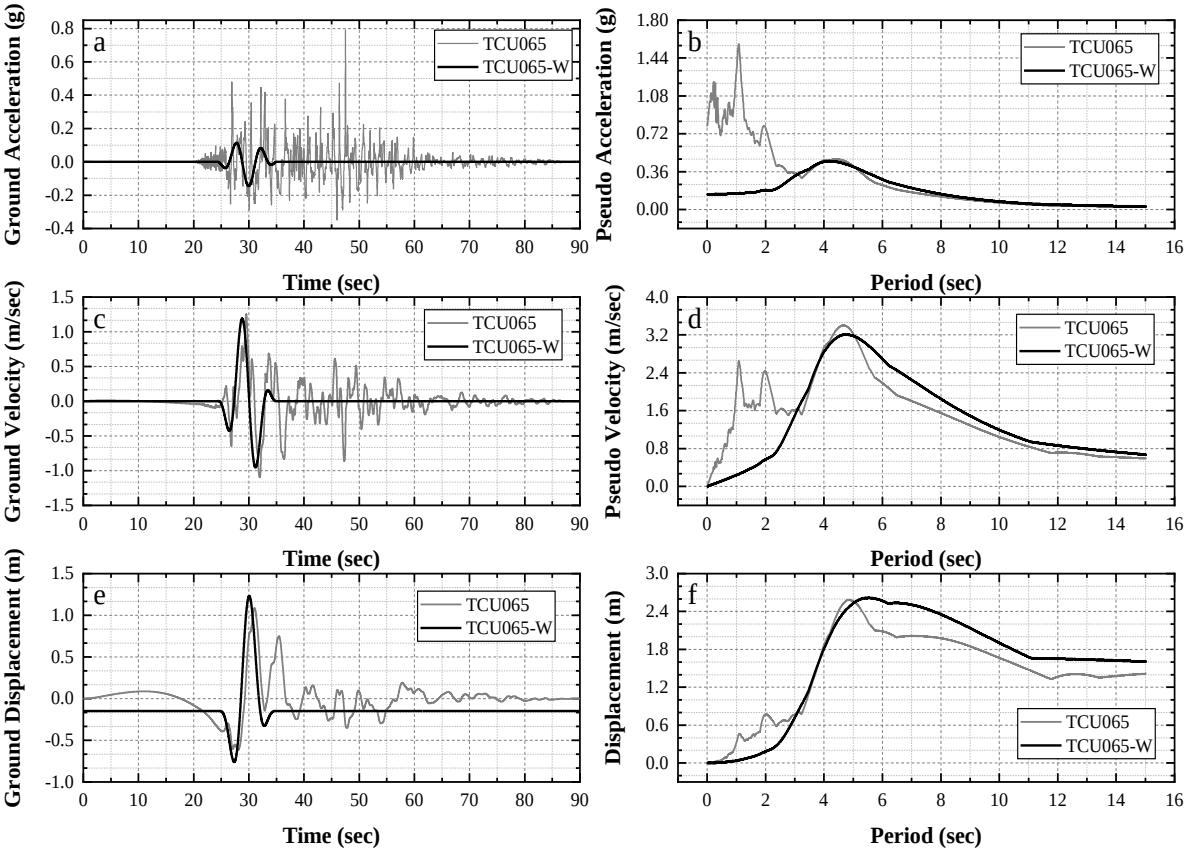

Figure 2: Comparison between actual and noise free long-period wavelet data adjusted to a Chi-Chi 1999 (TCU065) earthquake, along with their elastic response spectrum for 5% damping.

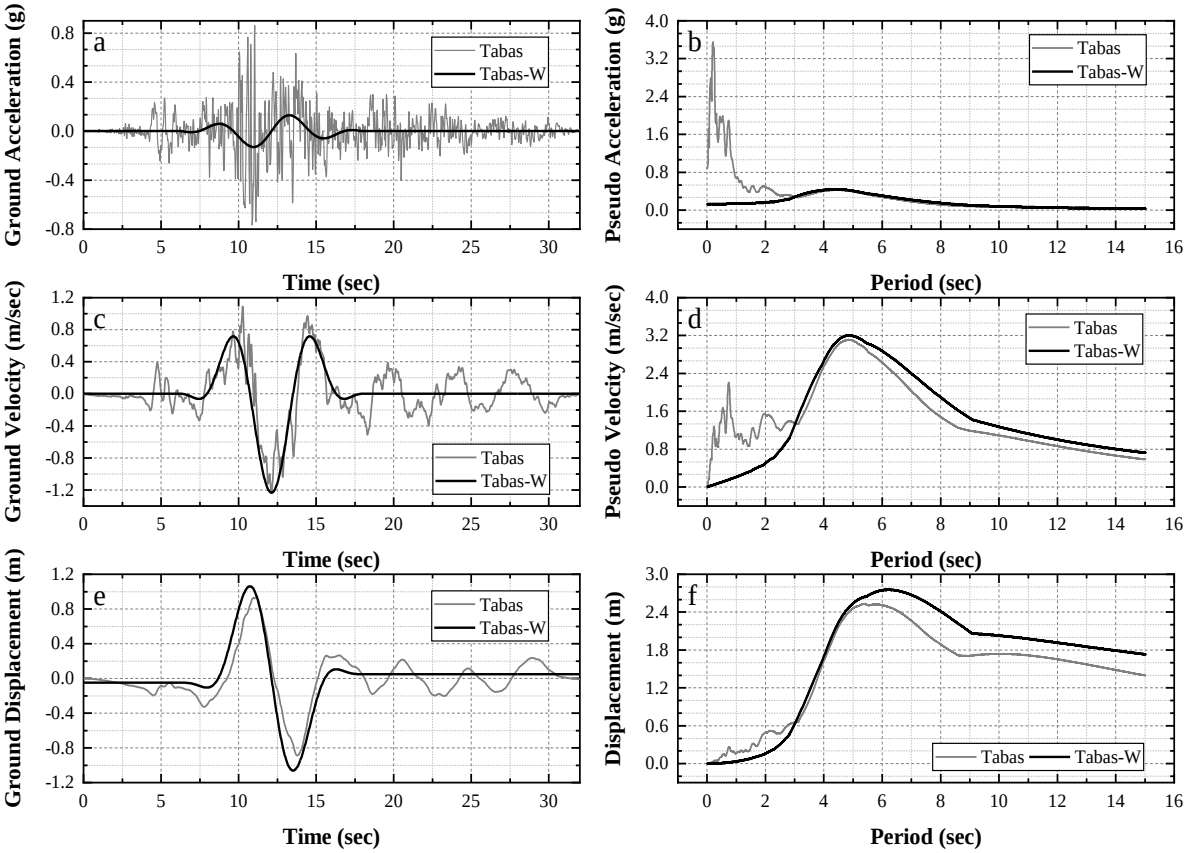

Figure 3: Comparison between actual and noise free long-period wavelet data adjusted to a Tabas 1978 earthquake, along with their elastic response spectrum for 5% damping.

$$T_i = \frac{2\pi d}{\sqrt{gb}} \tag{7}$$

The above-mentioned numerical model has been analysed using finite element software SAP2000. Currently, SAP2000 does not contain any numerical modelling package for VFPI, but recently Admane and Murnal (Admane and Murnal 2021) have

proposed a simplified modelling and analysis approach for VFPI by using SAP2000. Due to the simplicity of this approach than the specially developed stand-alone computer programs using programming languages, this study has used the finite element software SAP2000 for modelling and analysis of SDOF structure isolated by VFPI.

4. RESULTS AND DISCUSSION

In Section 2, the most destructive long-period wave of five distinct near-fault earthquakes (Table 1) are represented as a wavelet function (Table 2). In this section, the suitability of a noise-free long-period wavelet to replace a near-fault earthquake for an SDOF structure isolated by VFPI has been determined using three response quantities as indices: the base shear, the absolute acceleration of the top of the structure, and the sliding displacement at the isolator level. Using regression analysis, the structural responses such as base shear and the absolute acceleration at the top of structure have been depicted as a function of FVF.

4.1 Base Shear

Base shear is the most important parameter for the design of a structure. It represents the maximum expected lateral force on the structure due to seismic activity. The structural responses are mainly depending on the magnitude of base shear and therefore, seismic resistant design processes are mainly dependent on base shear. The base isolation system restricts the base shear up to a desirable limit so that the minimum lateral forces are involved in structural responses during an earthquake. In a base isolation system, the total isolator force directly acts as a base shear for the isolated structure. And in the case of the sliding isolator, the total isolator force is mainly divided into two parts: (1) frictional force, and (2) restoring force. Basically, the frictional force is depending on the coefficient of friction (μ) and it does not vary with the sliding displacement. Therefore, the variation of the isolator force in respect to the sliding displacement completely depends on the restoring force. Conceptually, the restoring force should be limited to a minimum value to take back the structure to its original position. But, in case of FPS, the restoring force is a linear function of the sliding displacement, and therefore FPS may develop high restoring force during near-fault earthquakes. This excessive restoring force ultimately increases the base shear for the isolated structure. While in the case of a VFPI, the restoring force sharply increases up to its peak value in the range of *0* to *0.58d* sliding displacement, after which the restoring force shows the softening behaviour. The peak restoring force of a VFPI decreases with increase in FVF value. So, the peak restoring force of the VFPI can be restricted up to a particular design value by properly selecting the FVF value. Due to this, the base shear of isolated structure can be restricted to a known value, which is not possible in the case of FPS.

The behaviour of the base shear of an SDOF structure isolated by VFPI (Section 3) under the five different actual earthquakes (Table 1), and extracted noise free long-period wavelets (Table 2) with respect to FVF values of *1* to *10* are shown in Figure 8. Under all the considered earthquakes apart from Gazil (USSR) 1976 earthquake (Figure 8(e)), the base shear response of the structure under the actual and extracted noise free long-period wavelets are closely matched with each other for all values of *FVF* (Figure 8(a), (b), (c), and (d)). Whereas in case of Gazil (USSR) 1976 earthquake, they are closely matched for *FVF* greater than or equal to 3, due to low *PGV* value or derived peak ground acceleration (a_g) (Table 3) of dominating long period wave of this earthquake. This derived peak ground acceleration (a_g) may be equal to the peak ground acceleration of the extracted noise free long-period wavelet and which is calculated from *PGV* and f_d of the parent earthquake. From the above discussion, it can be said that the extracted noise free long period wavelet effectively represents the near-fault earthquake in the case of base shear responses of the SDOF structure isolated by VFPI.

By observing Figure 8, the maximum base shear response of the considered structure isolated by VFPI under the extracted noise free long-period wavelet decreases exponentially with respect to the *FVF* values. Furthermore, it is found out that the "one-phase exponential decay function with *FVF* constant parameter" best fitted curve for representing the maximum base shear response for the structure and details of this function is given in equation (8), where, V_B is the maximum base shear ratio (maximum base shear normalised with weight of structure) for a particular value of *FVF*. Similarly, V_{mn} and V_{mx} are the maximum base shear ratios of the structure for very high (i.e., greater than 100) and very low (i.e., less than 0.00001) value of *FVF* respectively. According to the definition of parameter *V* in equation (9), it can be noted as the amplitude of the exponential equation (8). Therefore, the parameter FVF_c will become the *FVF* constant, and it is the *FVF* value at which the total reduction in *V* becomes 63%. The parameter discussed here is fully depending on the amplitude (*A*) and pulse frequency (f_p) of the extracted noise free long-period wavelet. Therefore, the parameters to fit the exponential curve (equation (8)) for the maximum base shear ratio of the structure isolated by VFPI under five different extracted noise free long-period wavelets (Table 2) have been found out by exponential regression analysis and are shown in Figure 8.

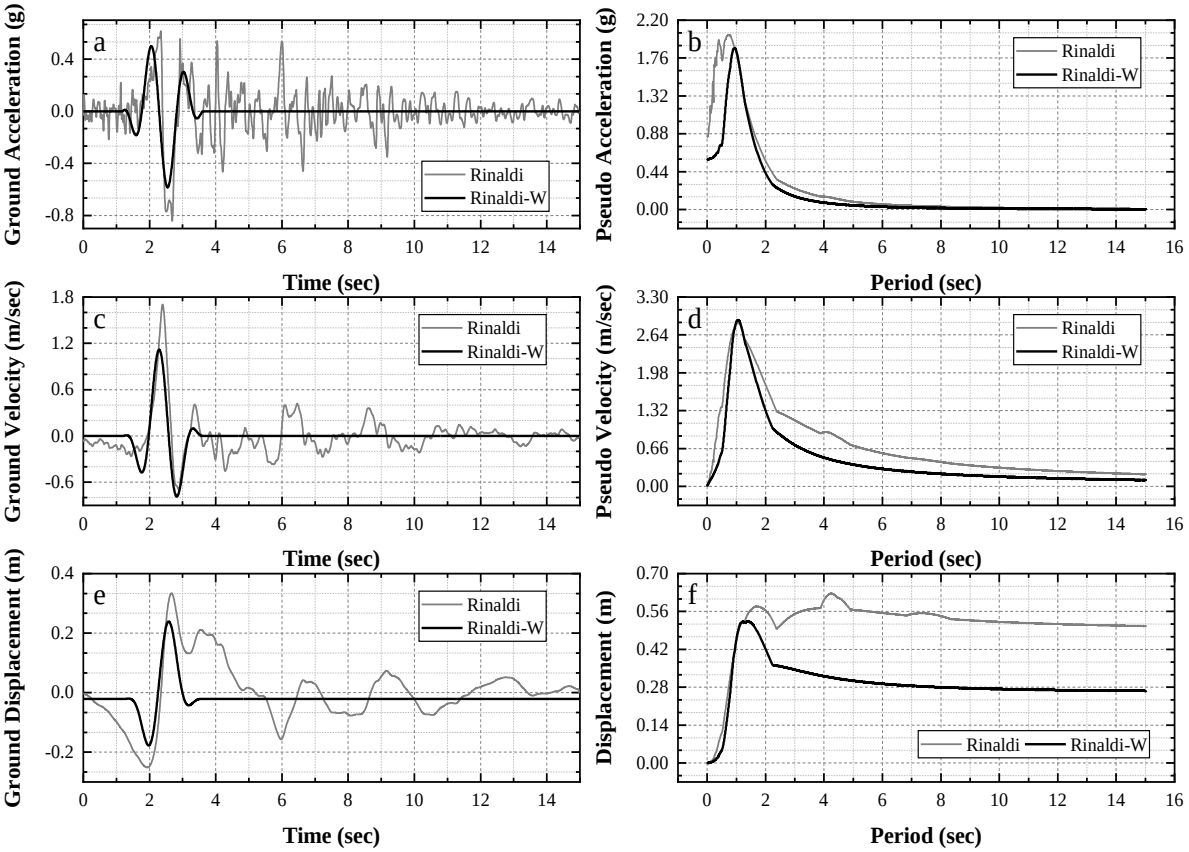

Figure 4: Comparison between actual and noise free long-period wavelet data adjusted to a Northridge 1994 (Rinaldi) earthquake, along with their elastic response spectrum for 5% damping.

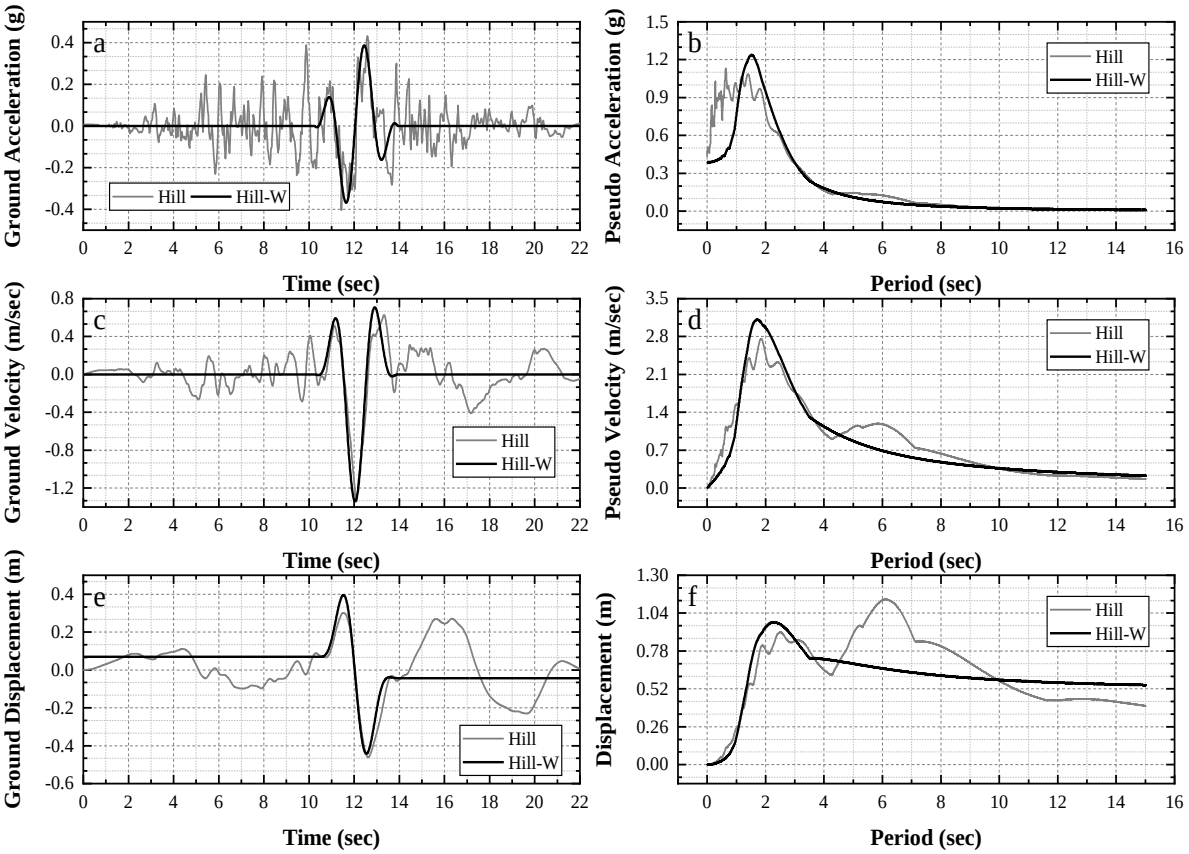

Figure 5: Comparison between actual and noise free long-period wavelet data adjusted to a Superstition Hills 1987 (Parachute Test Site) earthquake, along with their elastic response spectrum for 5% damping.

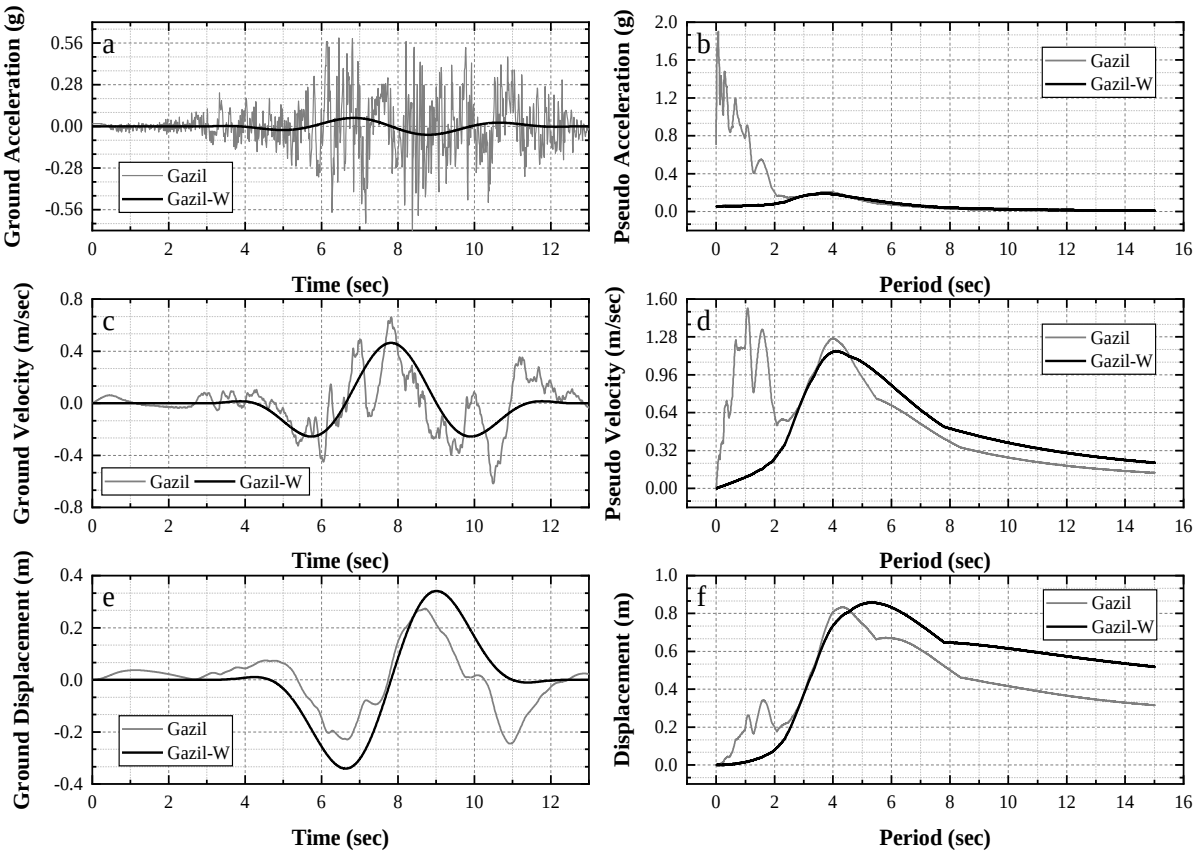

Figure 6: Comparison between actual and noise free long-period wavelet data adjusted to a Gazli 1976 (Karakyr) earthquake, along with their elastic response spectrum for 5% damping.

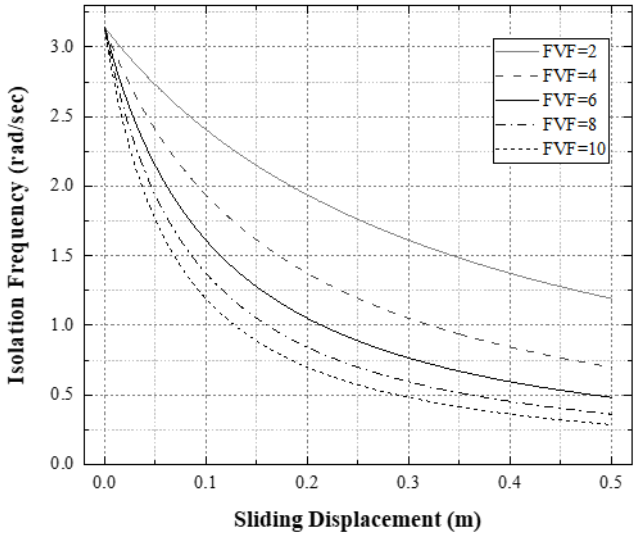

Figure 7: Impact of Frequency Variation Factor on isolation frequency of VFPI (T_i = 2.0 sec, μ = 0.02).

Table 3: Derived peak ground acceleration and displacement of five considered long period waves.

Earthquake Location	**f_p or f_d**	**A or PGV**	**Derived Peak Ground Acceleration (a_g)**	**Derived Peak Ground Displacement (x_g)**
(a)	(b)	(c)	$\frac{2\pi(b)(c)}{9.81}$	$\frac{(c)}{2\pi(b)}$
	(Hz)	**(m/s)**	**(g)**	**(m)**
Gazli, USSR	0.2100	0.4633	0.06231	0.35112
Tabas, Iran	0.1800	1.2334	0.14220	1.090565
Chi-Chi, Taiwan	0.1838	1.2500	0.14715	1.084817
Superstition Hills, CA, USA	0.4910	1.3422	0.42209	0.435067
Northridge, CA, USA	0.8281	1.1412	0.60528	0.21933

In Figure 8, the extension "F" used after every notation of an earthquake represents the best fitted curve for representing the maximum base shear ratio under the extracted noise free long-period wavelet of that earthquake. Similarly, the variation in V_{mn}, V and FVF_c with respect to derived peak ground acceleration (a_g) of extracting noise free long period wavelet is shown in Table 4. So, by using Table 4, the values of V_{mn}, V and FVF_c can be determined by interpolation of the required value of derived peak ground acceleration (a_g). Where, the derived peak ground acceleration (a_g) of long-period wave for a low frequency earthquake can be calculated by using its PGV and f_d value (Table 3).

$$V_B = V_{mn} + Ve^{-FVF/FVF_c} \tag{8}$$

$$V = V_{mx} - V_{mn} \tag{9}$$

Table 4: Variation of V_{mn}, V and FVF_c with respect to derived ground acceleration (a_g) of the synthetic long period wave for structure isolated by VFPI (T_i = 2.0 sec, μ = 0.02).

Peak Derived Ground Acceleration (a_g) (g)	V_{mn}	V	FVF_c (1/m)
0.06231	0.02660	0.09192	4.11331
0.14220	0.04006	0.27814	1.40194
0.14715	0.04007	0.27166	1.40094
0.42209	0.04007	0.27166	1.40093
0.60528	0.03946	0.24594	1.49977

4.2 Structural Acceleration

Acceleration and displacement of the structure are directly proportional to the magnitude of the base shear. Consequently, similar to base shear, the maximum absolute acceleration at the structure's top, which is isolated by VFPI, decreases as the FVF value increases under near fault earthquake and the extraction of noise-free long-period wavelets (Figure 9). Under all kinds of considered ground movements, the maximum absolute acceleration at the structure's top is within the allowed range and exhibits negligible variation in the FVF 5 to 10 range. From Figure 9, it can also be said that the structural response under the extracted noise free long-period wave closely matches with near-fault earthquakes for the structure isolated by VFPI. In other words, the noises free representation of a near fault earthquake can effectively be done by the extracted long period wavelet for the structure isolated by VFPI.

By carrying out some trial and error on the Figure 9, it has been found that the decrement flow of the maximum absolute acceleration at top of the structure isolated by VFPI under the extracted noise free long period wavelet as a ground motion follows the cubic pattern and details of this cubic function is given in equation (10), where, S_a denotes the structural absolute acceleration. Similarly, the parameters A_1, B_1, C_1 and D_1 are purely mathematical terms and have no physical meaning, but their values mainly depend on the amplitude (A) and the pulse frequency (f_p) of the extracted noise free long period wavelet. Therefore, the parameters to fit the above cubic expression (equation 10) for the maximum absolute acceleration at the top of the structure isolated by VFPI under five different extracted noise free long period wavelets have been found out by using cubic regression analysis and shown in Figure 9. Similarly, the variation in A_1, B_1, C_1 and D_1 with respect to derived peak ground acceleration (a_g) of extracted noise free long period wavelet is shown in Table 5. Like Table 4, Table 5 can also be used to determine approximate values of A_1, B_1, C_1 and D_1 from peak ground velocity (PGV) and dominating low frequency (f_d) of any low frequency earthquake.

$$S_a = A_1 + B_1(FVF) + C_1(FVF)^2 + D_1(FVF)^3 \tag{10}$$

Table 5: Variation of the A_1, B_1, C_1 and D_1 with respect to peak derived ground acceleration (a_g) of the synthetic long period wave for structure isolated by VFPI (T_i = 2.0 sec, μ = 0.02).

Peak Derived Ground Acceleration (a_g) (g)	A_1	B_1	C_1	D_1 (10^{-04})
0.06231	0.12425	-0.02345	0.00405	-2.25893
0.14220	0.27243	-0.05030	0.00375	-0.67130
0.14715	0.24491	-0.02741	0.00134	-0.18641
0.42209	0.34957	-0.07819	0.01078	-5.16639
0.60528	0.29161	-0.07022	0.00897	-4.02291

4.3 Sliding Displacement of VFPI

As discussed above, the main objective of the restoring force is to restore the original position of the structure and control the excessive sliding displacement of the isolator. It can be observed that, very small amount of restoring force is sufficient for taking back the structure to its original position and which has been maintained in VFPI for all sliding displacement (Pranesh and Sinha 2000). But due to the softening behaviour of the restoring force of VFPI, the isolator force generated under the long-period ground motions are not sufficient to control the excessive sliding displacement. Generally, the long period ground motion waves impose severe deformation demands at the isolator level.

Therefore, VFPI shows the excessive sliding displacement under some low frequency earthquakes. The amount of deformation demands at isolator level directly depends on the time-period of the long - period wave and its amplitude.

The variation in maximum sliding displacement of VFPI for 1 to 10 FVF values under actual ground motions and extracted noise free long period wavelets is shown in Figure 10. From Figure 10, it can be observed that the maximum sliding displacement of VFPI under extracted noise free long-period wavelets more closely match with parent near fault earthquakes. The small difference of maximum sliding displacement of VFPI under extracted noise free long-period wavelet and parent near fault earthquake may be due to the presence of high-frequency noises in parent near fault earthquake, and it may get involved in sliding displacement response due to the softening behaviour of restoring force in VFPI. It is clearly seen that the high-frequency noises over the dominating long period wave are higher in the case of the "Chi-Chi, Taiwan" and "Tabas, Iran" earthquake than other three earthquakes (Figure 2, Figure 3, Figure 4, Figure 5 and Figure 6); therefore, the difference in the maximum sliding displacement of VFPI under synthetic long-period wave and the actual low frequency earthquake are more in these two earthquakes (Figure 10). Northridge (Rinaldi), Gazil (Gazil), Superstition Hills (Hill), Chi-Chi (TCU065) and Tabas (Tabas) are sequences of the earthquakes which have been arranged on the basis of their derived peak ground displacement (x_g) of dominating time-period wave (Table 3) and the maximum sliding displacement (Figure 10). Therefore, it can be said that the maximum value of the sliding displacement of VFPI can be directly affected by derived peak ground displacement of the dominating low frequency wave of the earthquake. The derived peak ground displacement of dominating long period wave of Northridge (Rinaldi) and Gazil (Gazil) earthquakes are below 0.40 m (Table 3); and only for those two earthquakes, the VFPI shows the maximum sliding displacement below 0.50 m for any value of FVF (Figure 10). So, it can be said that the VFPI is likely to show excessive sliding displacement under those earthquakes which contain more than 0.40 m derived peak ground displacement of dominating long period waves. To verify this, the maximum sliding displacement (S_d) of VFPI under extracted noise free long period wavelets have been plotted against its derived peak ground displacement (x_g) for 1 to 10 values of FVF (Figure 11). From Figure 11, it can be observed that the maximum sliding displacement of VFPI suddenly increases near to 0.40 m derived peak ground displacement of extracted noise free long period waves.

4.4 Prediction of Responses

In the above section, it is found that the maximum base shear and maximum absolute acceleration of the structure isolated by VFPI can be effectively represented by the equation (8) and equation (10) respectively. Therefore, in this section, the capability of equation (8) and equation (10) to predict the structural responses such as maximum base shear ratio and maximum absolute structural acceleration of structure isolated by VFPI under low frequency earthquakes has been checked. For this purpose, the calculated and predicted structural and isolator responses of a SDOF structure isolated by VFPI (Section 3) under three different near fault ground motion (Table 6) have been compared. The predicted maximum base shear ratio and maximum absolute structural acceleration responses have been calculated from the equation (8) and equation (10) for 1 to 10 FVF values, respectively. For which, the required parameters to solve the equation (8) and equation (10) are interpreted from Table 4 and Table 5 for required value of derived peak ground acceleration of long period waves. For example, the derived peak ground acceleration value of Kocaeli, Turkey (1999) earthquake is 0.1307 g; therefore, the required parameters have been calculated from Table 4 and Table 5 by interpolation of 0.1307 g value in between 0.06231 g and 0.14220 g. The interpreted parameters for three different near fault earthquakes (Table 6) are given in Table 7. The maximum sliding displacement of VFPI has been calculated from Figure 11 for required value of derived peak ground displacement (Table 6).

Figure 12 shows the comparison between calculated and predicted structural and isolator responses of SDOF structure isolated by VFPI. Generally, the calculated and predicted maximum base shear responses closely match with each other for considered three near fault earthquakes for 1 to 10 FVF values. Whereas, the calculated and predicted maximum absolute structural acceleration and maximum sliding displacement responses show variation with each other; and this variation may be due to the involvement of the high-frequency noises in the structural responses. Apart from this variation, the predicted structural and isolator responses give an idea regarding the possible behaviour of the structure isolated by VFPI under near fault earthquake without analysing it.

5. CONCLUSION

This study has compared the performance of a SDOF structure isolated by VFPI of T_i = 2.0 s and μ = 0.02 under the five different low frequency earthquakes and their extracted noise free long-period wavelets. In addition, the effect of Frequency Variation Factor (FVF) of VFPI on the structural

and isolator responses were also investigated. The three-response quantity for this comparative study considered are the (1) base shear, (2) structural acceleration, and (3) isolator displacement.

The following conclusions can be drawn based on this investigation:

- The structural and isolator responses of the structure isolated by VFPI under the actual low frequency earthquakes closely match with their extracted noise free long-period wavelet. In other words, the Mavroeidis and Papageorgiou (Mavroeidis and Papageorgiou 2003) approach for extracting the noise free dominating low frequency wave of an earthquake can be suitable for the future study of structure isolated by VFPI.
- The structural responses such as the base shear and the structural acceleration under extracted noise free long-period wavelet as a ground motion follows the exponential and cubic function of FVF respectively.
- VFPI effectively restrict the structural responses within limits under all frequency earthquakes, but it may show the excessive sliding displacement for the earthquake which contains the derived peak ground displacement of long period wave more than 0.40 m.
- The high-frequency noises over the low frequency wave of an earthquake also contribute to the sliding displacement of VFPI due to its restoring force softening nature. Therefore, the response of a structure isolated by VFPI under two earthquakes having same amplitude and same time period of the long - period wave is always different.
- The proposed empirical formulas, chart, and tables give an idea about the possible behaviour of the structure isolated by VFPI by using the peak ground velocity (*PGV*) and dominating frequency (f_d) of the long period wave of a near fault earthquake.

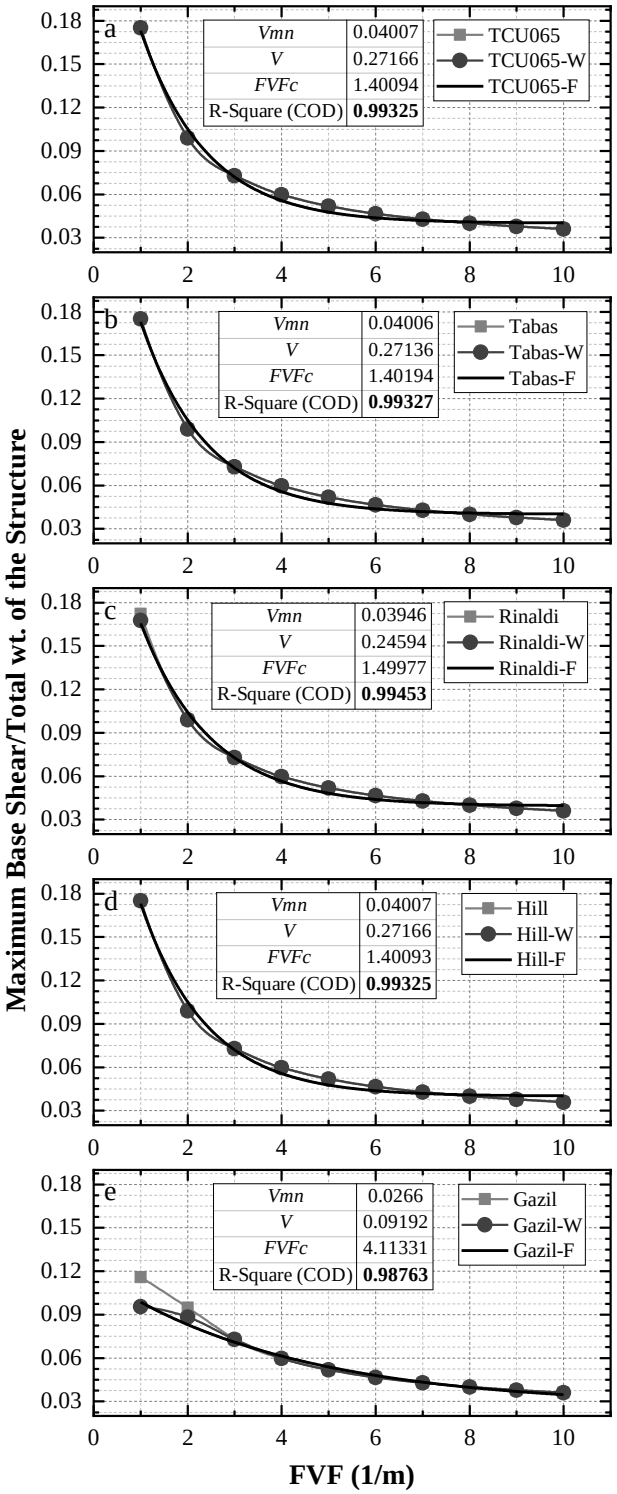

Figure 8: Comparison of base shear of a SDOF structure isolated by VFPI (T_i = 2.0 sec, μ = 0.02) under actual ground motion, extracted noise free long period wavelet, and best fitted curve.

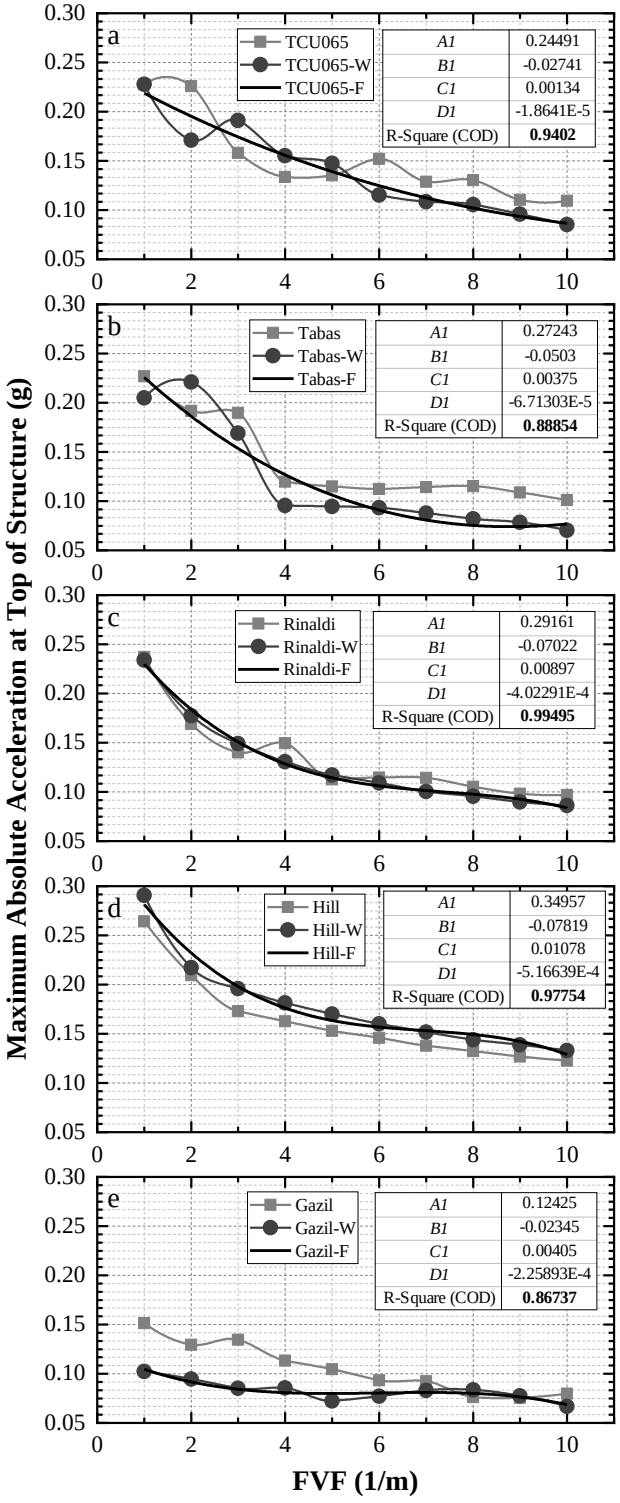

Figure 9: Comparison of absolute acceleration at top of a SDOF structure isolated by VFPI (T_i = 2.0 sec, μ = 0.02) under actual ground motion, extracted noise free long period wavelet, and best fitted curve.

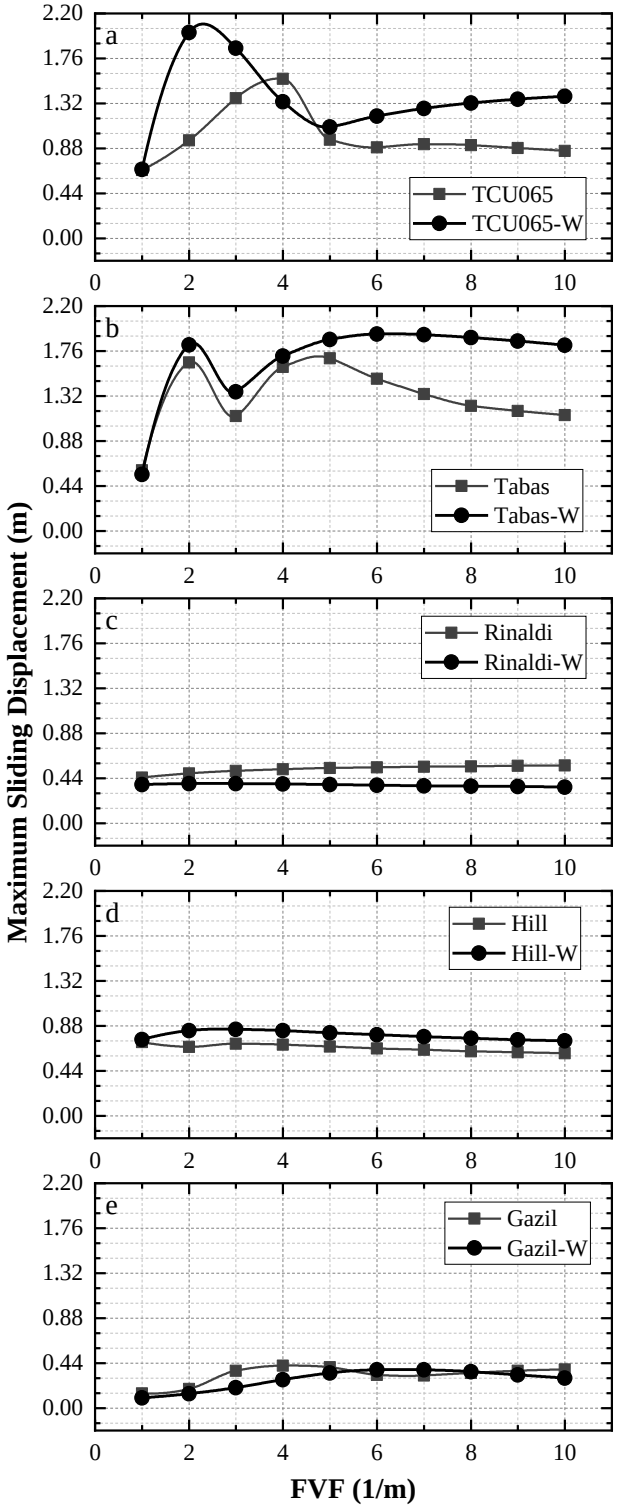

Figure 10: Variation in maximum sliding displacement of VFPI (T_i = 2.0 sec, μ = 0.02) under actual ground motions and extracted noise free long period wavelets.

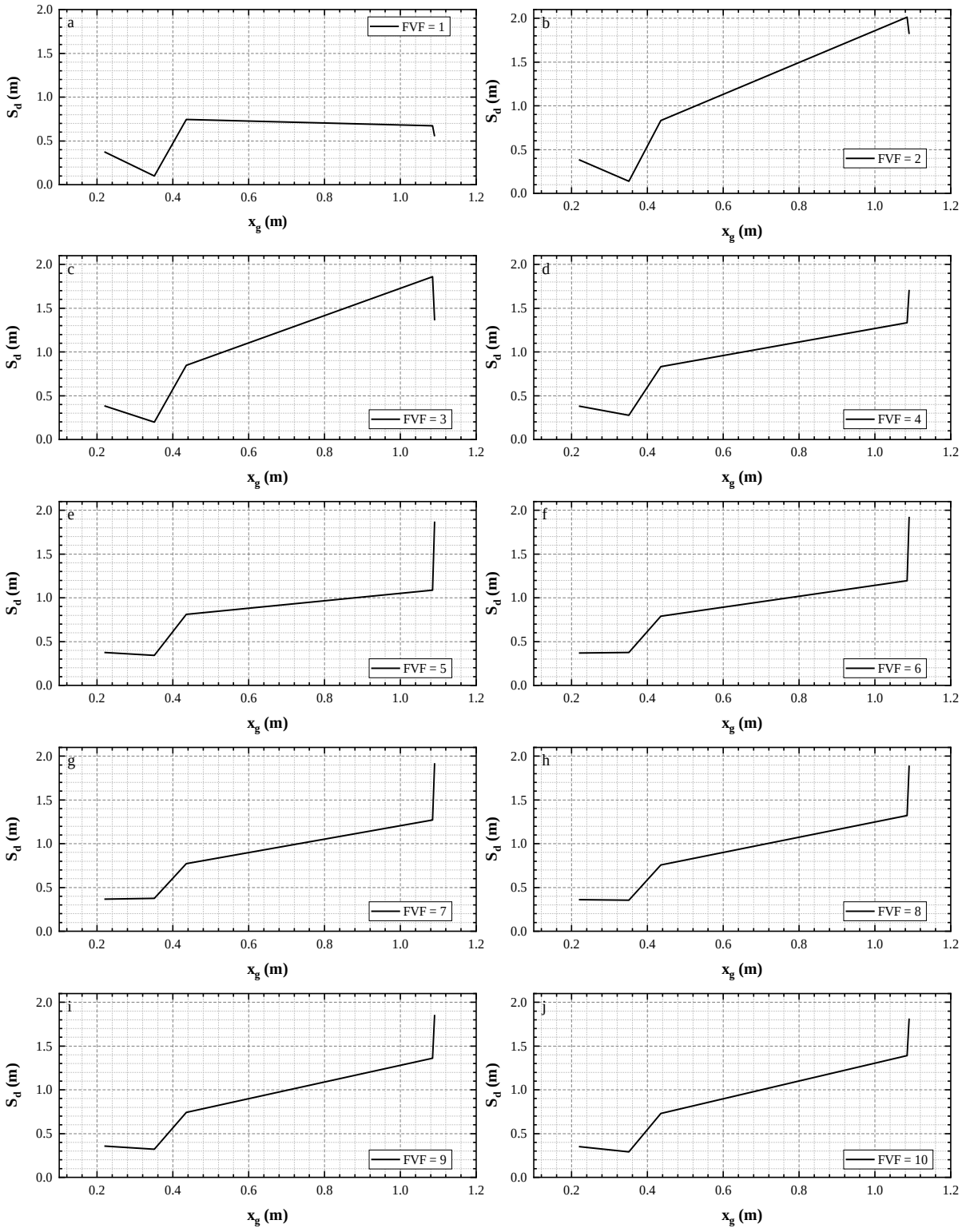

Figure 11: Variation in the maximum sliding displacement (S_d) of VFPI (T_i = 2.0 sec, μ = 0.02) with respect to derived peak ground displacement (x_g) of extracted noise free long period wavelet and frequency variation factor (FVF).

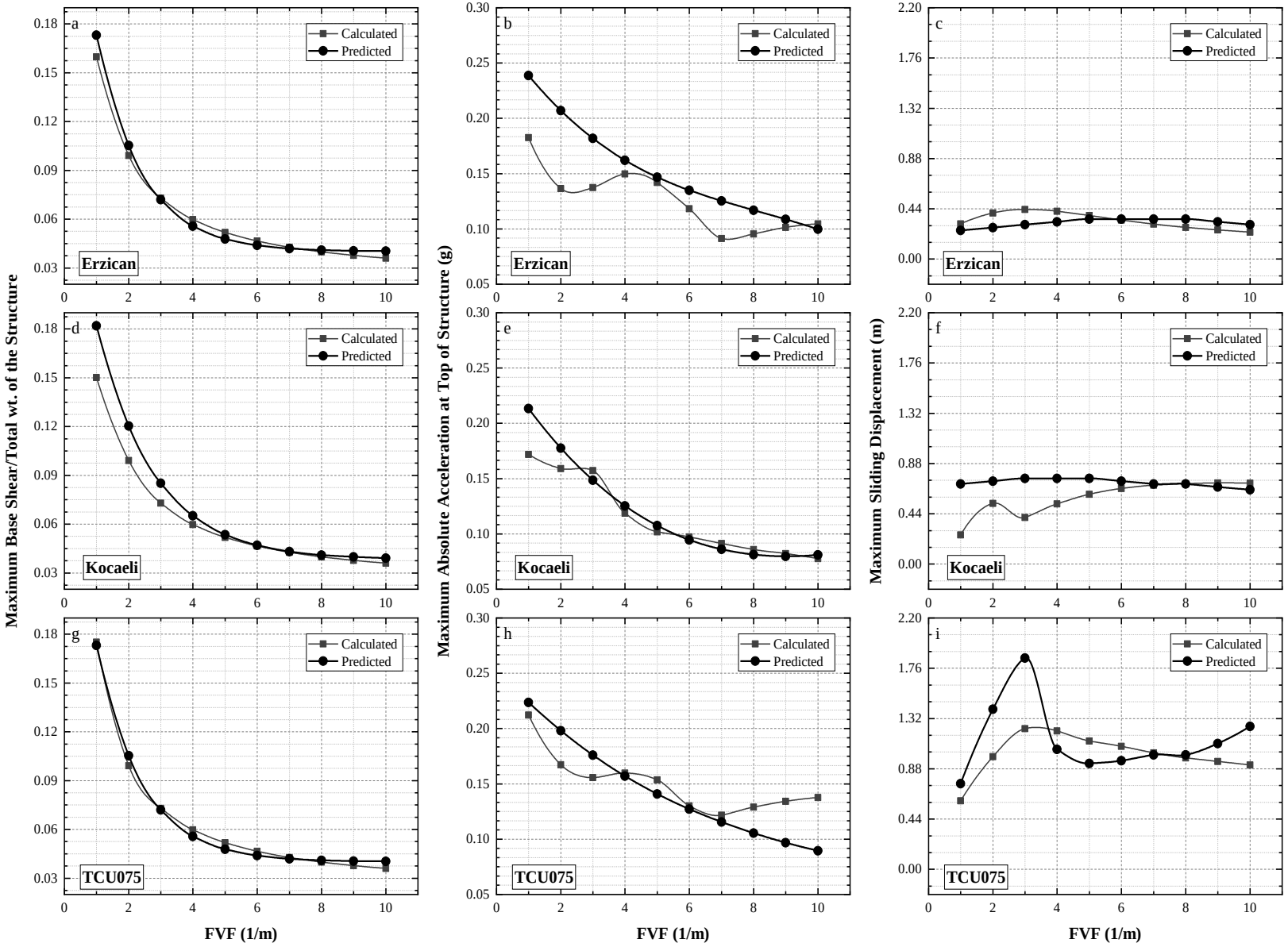

Figure 12: Comparison of calculated and predicted structural and isolator responses of structure isolated by VFPI (T_i = 2.0 sec, μ = 0.02).

Table 6: Near fault ground motion data used for prediction.

Sr. No.	Location	Year	Station	Recorded PGV (m/sec)	f_d (Hz)	Peak Derived Ground Acceleration, a_g (g)	Peak Derived Ground displacement, x_g (m)
1.	Erzican, Turkey	1992	Erzincan	0.7812	0.4673	0.2338	0.2661
2.	Kocaeli, Turkey	1999	Yarimca	0.7185	0.2841	0.1307	0.4025
3.	Chi-Chi, Taiwan	1999	TCU075	1.0947	0.2392	0.1677	0.7283

Table 7: Interpreted parameters for required peak derived ground acceleration (a_g).

Peak Derived Ground Acceleration (a_g) (g)	V_{mn}	V	FVF_c (1/m)	A_1	B_1	C_1	D_1 (10^{-04})
0.1307	0.03881	0.25143	1.79077	0.25601	-0.04645	0.00379	-0.89898
0.1677	0.04007	0.27166	1.40094	0.25275	-0.03121	0.00204	-0.55931
0.2338	0.04007	0.27166	1.40094	0.27789	-0.04341	0.00431	-1.75602

REFERENCES

Admane, H. A., and P. Murnal. 2021. "Comparative Analysis of SIVC Systems Using Simplified Analytical Modeling for Practical Design." *Pract. Period. Struct. Des. Constr.*, 26 (1): 04020051. https://doi.org/10.1061/(ASCE)SC.1943-5576.0000536.

Gabor, D. 1946. "Theory of communication. Part 1: The analysis of information." *J. Inst. Electr. Eng. - Part III Radio Commun. Eng.*, 93 (26): 429–441. https://doi.org/10.1049/ji-3-2.1946.0074.

Lu, L., M. Shih, and C. Wu. 2004. "Near-Fault Seismic Isolation Using Sliding Bearings With Variable Curvatures." *13th World Conf. Earthq. Eng.*, 3264–3278. Vancouver, B.C., Canada.

Malu, G., and P. Murnal. 2014. "Performance Evaluation of VFPI Subjected Near-Fault Ground Motion Through Wavelet Excitation." *SEC-2014*, 3136–3146. Delhi, India: Bloomsbury Publishing India Pvt Ltd.

Mavroeidis, G. P., and A. S. Papageorgiou. 2003. "A mathematical representation of near-fault ground motions." *Bull. Seismol. Soc. Am.*, 93 (3): 1099–1131. https://doi.org/10.1785/0120020100.

Murnal, P., and R. Sinha. 2002. "Earthquake Resistant Design of Structures using the Variable Frequency Pendulum Isolator." *J. Struct. Eng.*, 128 (7): 870–880. https://doi.org/10.1061/(ASCE)0733-9445(2002)128:7(870).

Murnal, P., and R. Sinha. 2004. "Behavior of Torsionally Coupled Structures with Variable Frequency Pendulum Isolator." *J. Struct. Eng.*, 130 (7): 1041–1054. https://doi.org/10.1061/(ASCE)0733-9445(2004)130:7(1041).

Panchal, V. R., and R. S. Jangid. 2008. "Seismic behavior of variable frequency pendulum isolator." *Earthq. Eng. Eng. Vib.*, 7 (2): 193–205. https://doi.org/10.1007/s11803-008-0824-9.

Pranesh, M., and R. Sinha. 2000. "VFPI: an isolation device for aseismic design." *Earthq. Eng. Struct. Dyn.*, 29 (5): 603–627. https://doi.org/10.1002/(SICI)1096-9845(200005)29:5<603::AID-EQE927>3.0.CO;2-W.

Shaikhzadeh, A. A., and A. Karamoddin. 2016. "Effectiveness of sliding isolators with variable curvature in near-fault ground motions." *Struct. Des. Tall Spec. Build.*, 25 (6): 278–296. https://doi.org/10.1002/tal.1258.

Tsai, C. S., T. C. Chiang, and B. J. Chen. 2003. "Finite element formulations and theoretical study for variable curvature friction pendulum system." *Eng. Struct.*, 25 (14): 1719–1730. https://doi.org/10.1016/S0141-0296(03)00151-2.

Zayas, V. A., S. S. Low, and S. A. Mahin. 1990. "A Simple Pendulum Technique for Achieving Seismic Isolation." *Earthq. Spectra*.